

# Nonparametric Aggregation of Geodesic Trends for Longitudinal Data Analysis

Kristen M. Campbell and P. Thomas Fletcher

Scientific Computing and Imaging Institute, University of Utah, Salt Lake City, UT

**Abstract.** We propose a technique for analyzing longitudinal imaging data that models individual changes with diffeomorphic geodesic regression and aggregates these geodesics into a nonparametric group average trend. Our model is specifically tailored to the unbalanced and sparse characteristics of longitudinal imaging studies. That is, each individual has few data points measured over a short period of time, while the study population as a whole spans a wide age range. We use geodesic regression to estimate individual trends, which is an appropriate model for capturing shape changes over a short time window, as is typically found within an individual. Geodesics are also adept at handling the low sample sizes found within individuals, and can model the change between as few as two timepoints. However, geodesics are limited for modeling longer-term trends, where constant velocity may not be appropriate. Therefore, we develop a novel nonparametric regression to aggregate individual trends into an average group trend. We demonstrate the power of our method to capture non-geodesic group trends on hippocampal volume (real-valued data) and diffeomorphic registration of full 3D MRI from the longitudinal OASIS data.

## 1 Introduction

Quantifying anatomical shape changes due to disease progression is an important step towards improving early disease detection, tracking treatment efficacy, and generally understanding disease processes. While cross-sectional studies have yielded some insights into disease progression, such as understanding atrophy in Alzheimer's, these methods cannot explain the changes that individuals undergo. Longitudinal studies, on the other hand, measure changes within individuals by repeating measurements for each participant over time. This allows estimation of individual trajectories, as well as the average trajectory for a group.

Semiparametric mixed effect models have been used to analyze longitudinal data such as height changes over time [3]. These mixed effect models have been used to analyze longitudinal neuroimaging data by looking at summary measures like volume of the brain or its various substructures. However these summaries cannot give a detailed picture of where or how the shape changes over time. Other methods have extended this analysis to look at longitudinal change of substructure surfaces [12, 17]. This requires segmenting the structures of interest beforehand and finding correspondences between points on the surface. Work

has also been done to analyze longitudinal change of measures like fractional anisotropy along DTI fiber tracts [18]. Allowing the measures to vary along the tracts is valuable, but it requires measurements along the length of the tract and alignment of tracts across subjects. In fact, many of the existing methods are designed to work with this kind of balanced data where all subjects have measurements across the entire duration of the period of interest.

Some analysis has been done on longitudinal univariate manifold data, in particular trying to find alignment of time of disease onset [14]. We want to go beyond the univariate measures and characterize shape changes over time. Methods for looking at shape change over time [4, 10, 5, 8] look for geodesic group trends and geodesic subject trends. However, as pointed out in [7], a geodesic model is not sufficient to explain shape change during periods of significant growth or atrophy. This is because a geodesic must be constant velocity, whereas anatomical shape changes typically exhibit acceleration or deceleration.

We develop a longitudinal data analysis that has the flexibility to model complex, non-constant speed trends at the group level. At the same time, we can handle individual data that is sparsely sampled in time, and unbalanced, that is, individuals are not sampled at the same timepoints, and may even have different numbers of measurements. To do this, we model the individual trends with a geodesic, which is adept at sparsely sampled, short-term shape trends. Next, we develop a novel method called Aggregation of Longitudinal Geodesics (ALG) for averaging the geodesic trends into a nonparametric group trend that can capture accelerating or decelerating shape changes. We perform experiments with 3D brain MRI and associated univariate measurements to show that the group trends are not constant speed and that our approach captures these complexities.

## 2 Methods

We consider longitudinal data lying on a Riemannian manifold  $M$ . In the present paper, we will analyze univariate measurements ( $M = \mathbb{R}$ ), as well as 3D MR images under the LDDMM metric. However, our method is generally applicable to other manifolds. Let  $y_{ij} \in M$  denote the  $j$ th measurement from the  $i$ th subjects, taken at time  $t_{ij}$ , and let  $N$  be the number of subjects, each with  $P_i$  measurements. The full data set spans an age range,  $[t_{\min}, t_{\max}]$ , while each individual subject spans a much smaller age range, i.e.,  $t_{i,P_i} - t_{i,1} \ll t_{\max} - t_{\min}$ .

**Individual Geodesic Trends.** We start by modeling the subject-specific trajectories as geodesic curves,  $\gamma_i : [t_{i1}, t_{iP_i}] \rightarrow M$ . These geodesic trends are fit to the subject data,  $(t_{ij}, y_{ij})$  using geodesic regression. A geodesic can be parameterized by its initial position  $p = \gamma_i(t_{i1}) \in M$  and velocity  $v = \gamma'_i(t_{i1}) \in T_p M$  (tangent space to  $p$ ). Geodesic regression [6] solves the least-squares problem:

$$(\hat{p}_i, \hat{v}_i) = \arg \min_{(p,v) \in TM} d(y_{ij}, \text{Exp}_p(t_{ij}v))^2,$$

where  $\text{Exp}$  is the Riemannian exponential map, which converts an initial position and velocity into a geodesic curve, i.e.,  $\gamma(t) = \text{Exp}_p(tv)$ , and  $d(\cdot, \cdot)$  is the

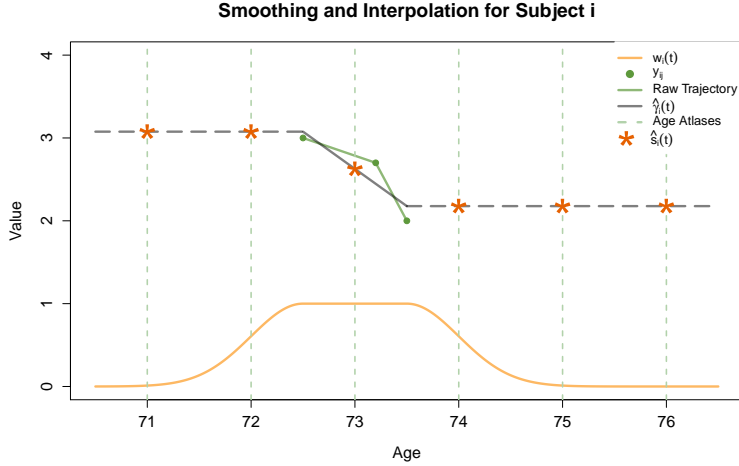


Fig. 1: Illustration showing the contributions from one subject’s longitudinal measurements, weighted by the kernel function  $w_i(t)$ .

Riemannian distance on  $M$ . The end result, for each subject  $i$ , is an estimated geodesic trend  $\hat{\gamma}_i$ , parameterized by its initial position  $\hat{p}_i$  and velocity  $\hat{v}_i$ .

For univariate data, a geodesic is a straight line, and geodesic regression is simply ordinary least-squares regression. Whereas, for images, we use diffeomorphic geodesic regression [11]. For this work, we used the vector momenta formulation [15] of LDDMM to perform the geodesic regression. In order to define kernel-weighted averaging of trends, we need a definition of an individual’s trend over time extending for the full support of the kernel, which will generally extend beyond the time interval of a subject. To do this, we define a constant extension of the data at the endpoints for a subject. Thus, the  $i$ th subject’s trend is given by

$$\hat{s}_i(t) = \begin{cases} \hat{\gamma}_i(t_{i1}) & \text{if } t < t_{i1}, \\ \hat{\gamma}_i(t) & \text{if } t_{i1} \leq t \leq t_{iP_i}, \\ \hat{\gamma}_i(t_{iP_i}) & \text{otherwise.} \end{cases} \quad (1)$$

**Nonparametric Group Trend.** We build a group trend of age-specific atlases as a nonparametric kernel regression of the subject-specific models’ predictions. We then compute a weighted average of the data (univariate or images) at that age where the weight for a subject’s interpolated image is 1 when the age falls between the time of the first and last measurement for that subject. Outside of that window, the weight for an age,  $t$ , decreases according to a Gaussian kernel of the form

$$K_l(t, i) = e^{-\frac{(t-t_{i,1})^2}{2\sigma^2}}, K_r(t, i) = e^{-\frac{(t-t_{i,P_i})^2}{2\sigma^2}} \quad (2)$$

where  $K_l(t, i)$  is used when age  $t < t_{i,1}$  and  $K_r(t, i)$  is used when the age  $t > t_{i,P_i}$ . These kernels are used to compute the weight function,  $w_i$  for each subject:

$$w_i(t) = \begin{cases} K_l(t, i) & \text{if } t < t_{i,1}, \\ 1 & \text{if } t_{i,1} \leq t \leq t_{i,P_i}, \\ K_r(t, i) & \text{otherwise.} \end{cases} \quad (3)$$

To construct an age atlas,  $a_t$ , at age  $t$ , we compute the weighted Fréchet mean:

$$a_t = \arg \min_{a \in M} \sum_{i=1}^N w_i(t) d(\hat{s}_i(t), a)^2. \quad (4)$$

For univariate data ( $M = \mathbb{R}$ ), the solution to this minimization problem is the weighted average. For images under the LDDMM metric, we follow the approach in [2], by constructing the weighted diffeomorphic atlas  $a_t$  by gradient descent optimization. In Figure 1, we illustrate how one subject would contribute to the age atlases constructed every year between 71 and 76.

### 3 Experiments

#### 3.1 Simulated Univariate Data

Before applying ALG to real data, we wanted to understand how well it can reconstruct a known nonlinear group trend in longitudinal data. We start by simulating univariate data with a ground truth group trend of  $y = 4x^2 - 8x + 4$  in the range  $[0, 1]$  with slope  $y' = 8x - 8$ . We simulate longitudinal data for  $N = 100$  subjects by generating  $P_i = 3$  time points for each subject that follow a noisy  $y$ -shifted version of the group trend. We draw the middle age for a subject,  $t_{i,2} \sim \text{Unif}(0, 1)$ , and compute the group slope and intercept at this point. We then choose a random first and last age not too far away in time,  $t_{i,1} = t_{i,2} - \delta_{i,1}, t_{i,3} = t_{i,2} + \delta_{i,2}$  where  $\delta_{i,j} \sim N(0, 0.05)$ . From these time points we generate the associated measurements  $m_{i,j} = y'(t_{i,2}) * t_{i,j} + y(t_{i,2}) - y'(t_{i,2}) * t_{i,2} + \eta_i + \epsilon_{i,j}$  where  $\eta_i \sim N(0, 1)$  and  $\epsilon_{i,j} \sim N(0, 0.1)$ .

We apply ALG with  $\sigma = 0.1$  for 10 equally spaced age atlases,  $a_t$ . Figure 2 shows all 100 subjects and the age atlases showing the estimated group trend. Notice that the estimated group trend closely follows the nonlinear ground truth trend.

#### 3.2 Simulated Images

We tested ALG with simulated images by creating a longitudinal version of the cross-sectional bulls-eye experiment from [2]. We generate 256x256 2D bulls-eye images at 4 different time points for each of 173 individuals where the 3 radii that define each bulls-eye evolve in time according to known processes. The innermost radius,  $R_1$ , follows a logistic decay process from 18 pixels at age 65 to 12 at age

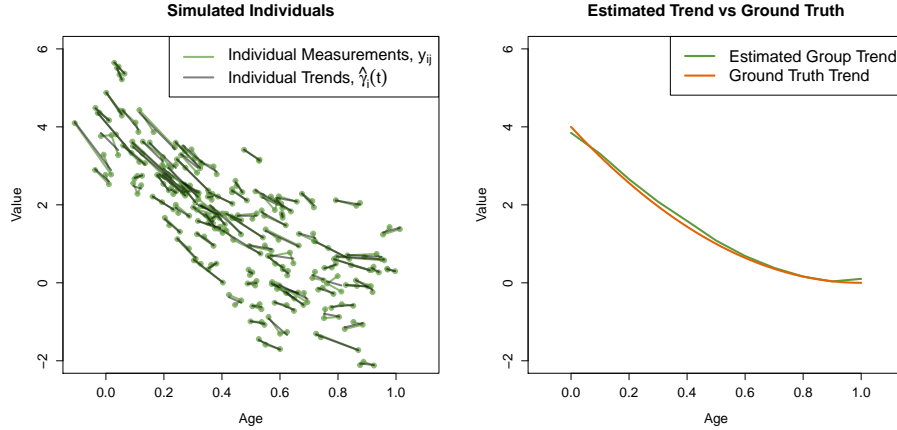


Fig. 2: Left: longitudinal data simulated to follow a nonlinear group trend. Right: atlas values computed by ALG recover the ground truth trend.

95. The middle radius,  $R2$ , grows logistically from 25 to 45 pixels over the same time, and the outer radius,  $R3$ , grows linearly from 70 to 90 pixels.

The starting age for the  $i$ -th subject is drawn from  $t_{i,0} \sim \text{Unif}(0, 1)$ . The ages for each of the subsequent 3 time points for that subject are  $t_{i,j+1} = t_{i,j} + \delta_{i,j}$  where  $\delta_{i,j} \sim N(1, 0.5)$ . The radii for the  $i$ -th subject at the  $j$ -th time point are calculated as

$$R_{1,i,j}(t_{i,j}) = f_1(t_{i,j}) + \eta_{1,i} + \epsilon_{1,i,j} \quad (5)$$

$$R_{2,i,j}(t_{i,j}) = f_2(t_{i,j}) + \eta_{2,i} + \epsilon_{2,i,j} \quad (6)$$

$$R_{3,i,j}(t_{i,j}) = f_3(t_{i,j}) + \eta_{3,i} + \epsilon_{3,i,j}, \quad (7)$$

where the  $k$ -th radius has a subject-specific noisy shift,  $\eta_{k,i} \sim N(0, 2)$ , and also timepoint-specific noise,  $\epsilon_{k,i,j} \sim N(0, 1)$ . Once the images are created, zero-mean Gaussian noise with standard deviation = 0.03 is added to the image intensities.

Figure 3 shows the results of univariate ALG with  $\sigma = 3$  performed separately on each of the radii measurements to create an age atlas for each year between 65 and 95. We then apply ALG with the same sigma value to the 173 sets of 4 longitudinal 2D images (see Figure 4 for a representative selection of these images). As shown in Figure 5, we compared the estimated atlases and associated momenta with the ground truth atlases and found that the original atlases are recovered and that the momenta between atlases change nonlinearly over time.

To quantify the dynamics of the shape change, we looked at two properties of the estimated paths: the norm of the momenta at each time point and also the deviation of the velocity from a geodesic (see Figure 6). A geodesic satisfies the equation,  $\frac{dv}{dt} + \text{ad}_v^\dagger v = 0$ . So, if we compute the left-hand side, we can measure how “non-geodesic” the path is, and we call this value the curvature of the path.

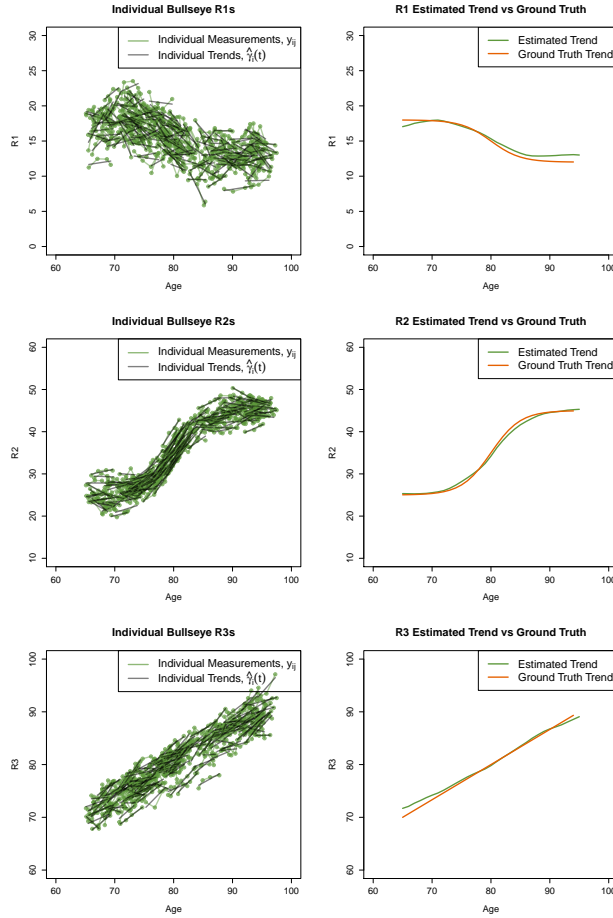


Fig. 3: Univariate ALG analysis of bulls-eye radii.

This is the covariant derivative of the velocity along the path, i.e.,  $\nabla_{v(t)}v(t)$ . If the norm is nearly constant and the curvature is nearly 0 everywhere then the longitudinal trend is linear. Notice that our results have a large increase in both the norm and curvature around age 80, consistent with the logistic processes for R1 and R2 that change the fastest at their halfway point. ALG successfully models this nonlinear group trend in the image data and provides atlases for each age that match the ground truth image for that age.

### 3.3 Real Data

We used T1 MRIs for 142 adults with and without Alzheimer’s disease from the longitudinal OASIS database [9] with 72 Nondemented (Clinical Dementia Rating, CDR = 0) subjects between the ages of 60 and 93, 56 Demented (CDR

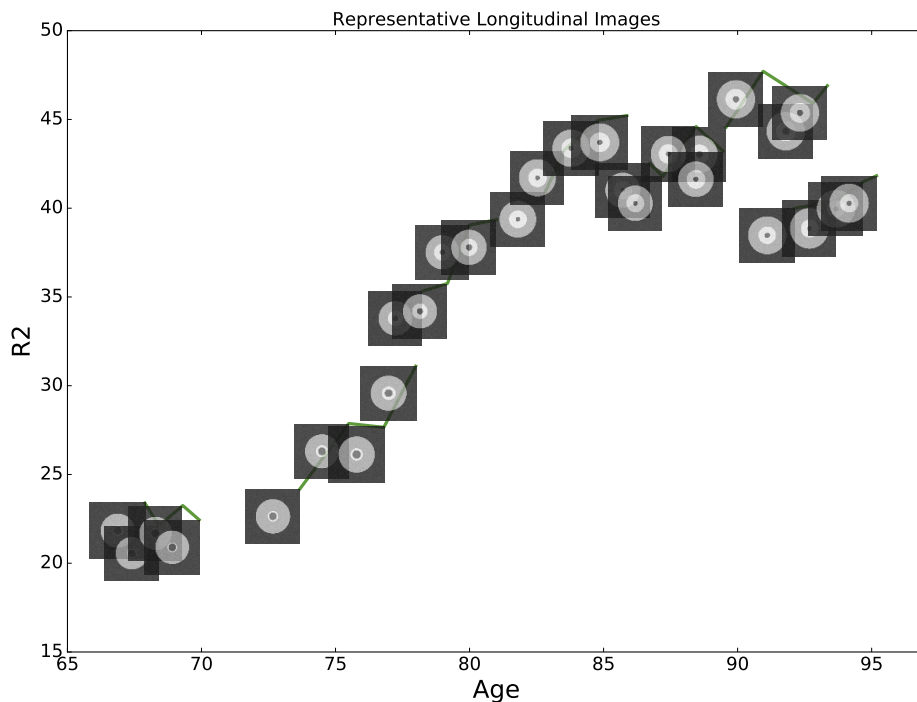


Fig. 4: A representative selection of individuals from the longitudinal bulls-eye data.

$\geq 0.5$ ) subjects between the ages of 61 and 96 and 14 Converted subjects (CDR changed from 0 to 0.5 over course of the study) between the ages of 65 and 87. The subjects had between 1 and 5 MRI scans taken with a time between first and last scans of between 1 and 7 years.

All images were processed using longitudinal Freesurfer to do skull stripping and intensity normalization and to measure left and right hippocampal volumes [13]. Geodesic regression was then performed on the processed images for each subject individually as described in [16]. We use the vector momenta implementation of geodesic shooting to shoot the initial momenta from the individual geodesic regressions in order to find an image for a subject at a particular age. We chose to use the “Goldie Locks” sigma of 6 years for the kernel which was also used by [2].

First, we look at the left and right hippocampal volumes computed by longitudinal Freesurfer. Figure 7 shows the results of ALG applied to left hippocampal volumes normalized by inter-cranial volume (ICV). Similar results were found for the right hippocampus. Note in particular that our method captures the nonlinear nature of the volume change over time.

Now let’s look how the diffeomorphisms change over time. In Figure 8, we show the age atlases overlaid with the initial momenta at each age. Notice that

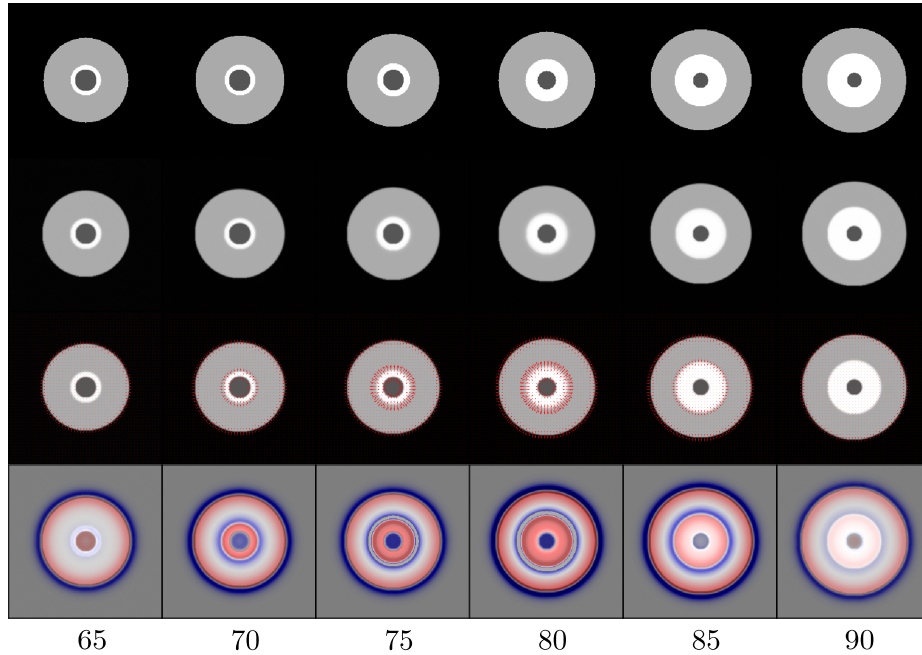


Fig. 5: Columns 1-6: 2D bullseye atlases at a selection of ages. First row: Ground truth images. Second row: Estimated atlases. Third row: Estimated atlases with initial momenta overlaid as red arrows. Last row: Estimated atlases with the log jacobian determinant of the deformations from one atlas to the next overlaid. Blue is contraction (negative values), white is 0 and red is expansion (positive values).

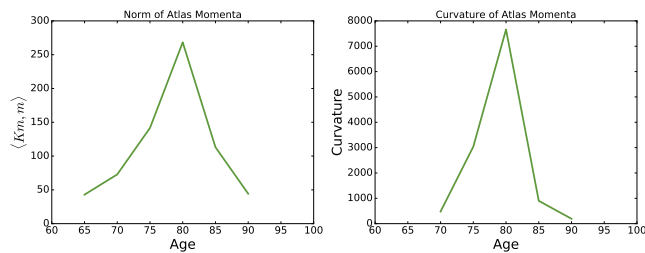


Fig. 6: Momenta norm and curvature of estimated bulls-eye atlases.

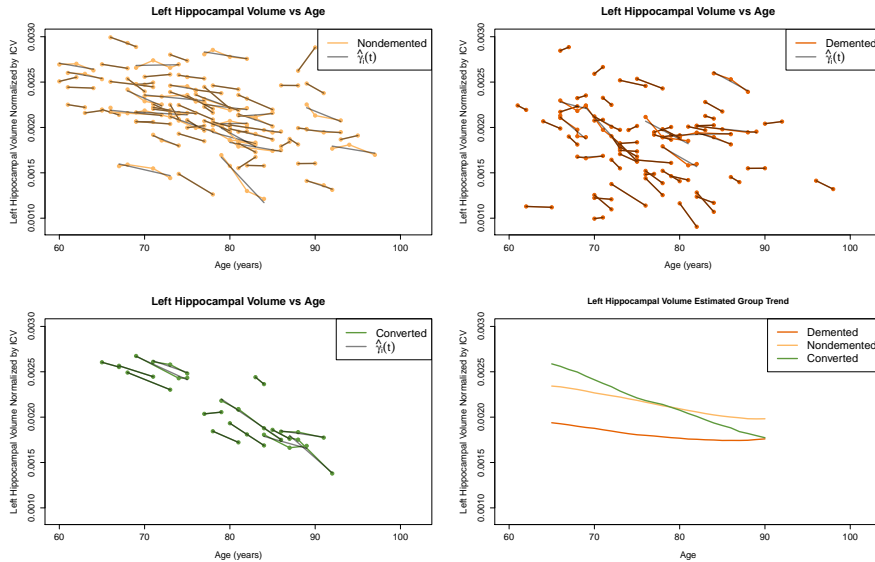


Fig. 7: Left hippocampal volumes normalized by inter-cranial volume (ICV).

the location and magnitude of the shape change changes over time, especially around the ventricles and hippocampi. This is consistent with the literature [1, 12, 17]. We quantified this nonlinearity by computing the norm and curvature of the momenta between estimated atlases as shown in Figure 9. Since the norm is nonconstant and the curvature is nonzero, the shape change of these images is nonlinear. The age-specific atlases generated by ALG capture this acceleration and deceleration in shape change over time.

## 4 Discussion

We presented ALG, a method that can aggregate longitudinal measurements across subjects, where the measurements for an individual span a small time window compared to the aggregated time window. ALG works for any manifold data that can be modelled by a geodesic regression.

We applied ALG to simulated univariate and image data and were able to recover the underlying group trend in both cases. We then applied ALG to the longitudinal OASIS data and saw that the group trends for atrophy are nonlinear, with different structures atrophying at different rates and different times in the disease progression, which is consistent with the literature [1]. This demonstrates that ALG is indeed able to capture accelerating and decelerating anatomical shape changes.

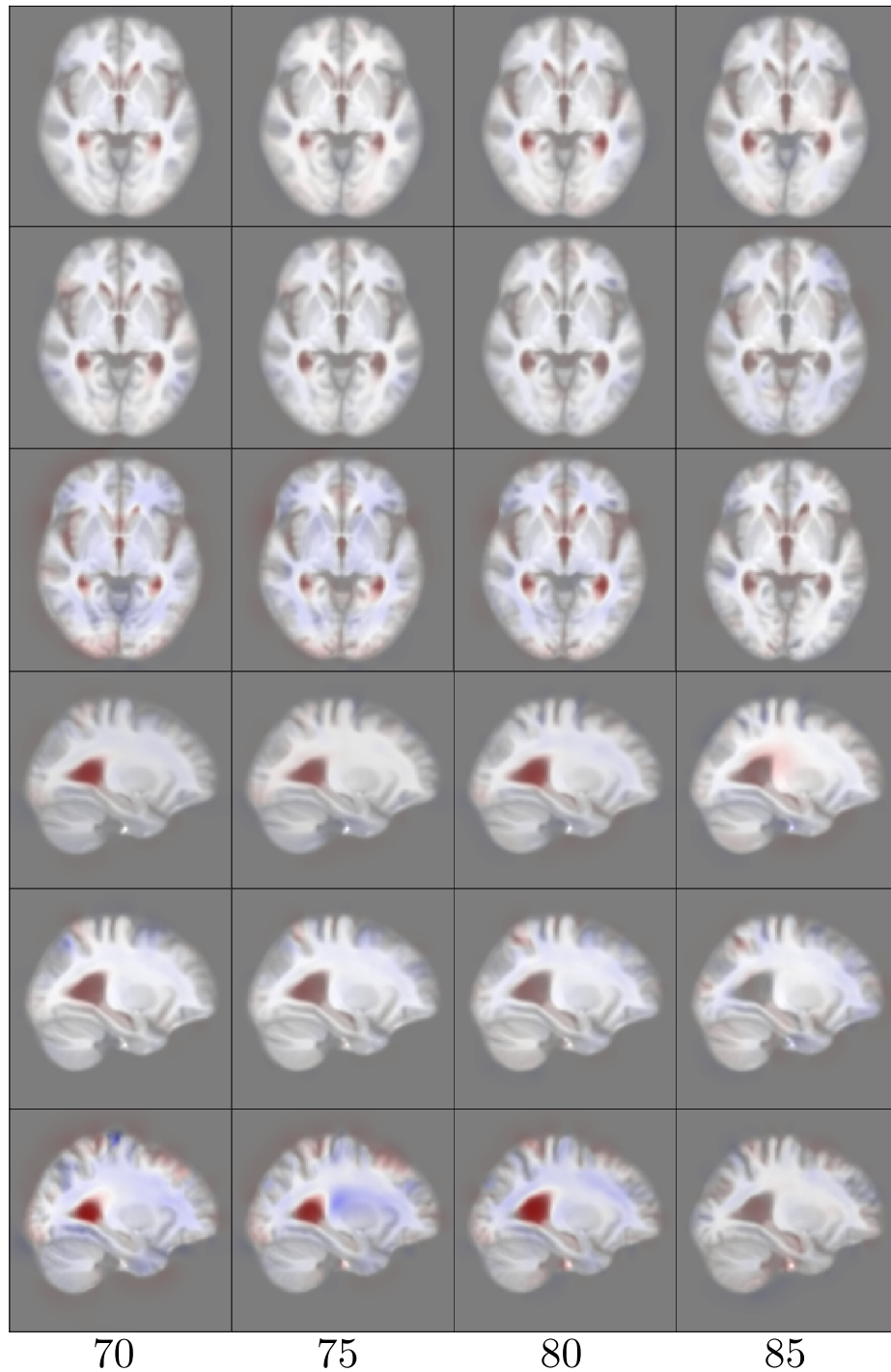


Fig. 8: Columns 1-4: atlases of 3D OASIS data at a selection of ages. Rows 1-3: 2D axial view of Nondemented, Demented and Converted atlases respectively. Rows 4-6: 2D sagittal view of Nondemented, Demented and Converted atlases respectively. The log jacobian determinant of the deformations from one atlas to the next are overlaid with a colormap, where blue is contraction, white is 0 and red is expansion.

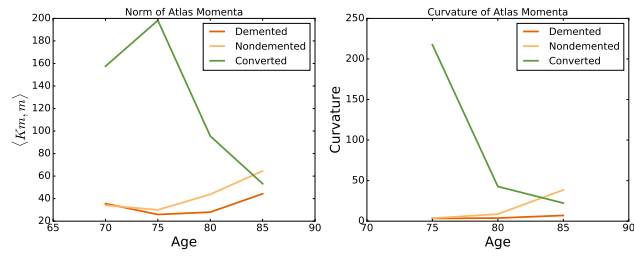


Fig. 9: Momenta norm and curvature of OASIS atlases.

**Acknowledgements** This work was supported by NIH grant R01EB022876. The OASIS data was provided by the following grants: P50 AG05681, P01 AG03991, R01 AG021910, P20 MH071616, U24 RR021382. Thanks to Nikhil Singh for providing the preprocessed Freesurfer data and subject-specific geodesic regressions.

## References

1. Braak, H., Braak, E.: Evolution of the neuropathology of alzheimer's disease. *Acta Neurologica Scandinavica* **94**(S165), 3–12 (1996)
2. Davis, B., Fletcher, P., Bullitt, E., Joshi, S.: Population shape regression from random design data. *International journal of computer vision* **90**(2), 255–266 (2010)
3. Durbán, M., Harezlak, J., Wand, M., Carroll, R.: Simple fitting of subject-specific curves for longitudinal data. *Statistics in medicine* **24**(8), 1153–1167 (2005)
4. Durrleman, S., Pennec, X., Trounev, A., Braga, J., Gerig, G., Ayache, N.: Toward a comprehensive framework for the spatiotemporal statistical analysis of longitudinal shape data. *International journal of computer vision* **103**(1), 22–59 (2013)
5. Fishbaugh, J., Prastawa, M., Durrleman, S., Piven, J., Gerig, G.: Analysis of longitudinal shape variability via subject specific growth modeling. In: MICCAI. pp. 731–738. Springer (2012)
6. Fletcher, T.: Geodesic regression on riemannian manifolds. In: MFCA. pp. 75–86 (2011)
7. Gerig, G., Fishbaugh, J., Sadeghi, N.: Longitudinal modeling of appearance and shape and its potential for clinical use. *Medical image analysis* **33**, 114–121 (2016)
8. Hadj-Hamou, M., Lorenzi, M., Ayache, N., Pennec, X.: Longitudinal analysis of image time series with diffeomorphic deformations: a computational framework based on stationary velocity fields. *Frontiers in neuroscience* **10**, 236 (2016)
9. Marcus, D., Fotenos, A., Csernansky, J., Morris, J., Buckner, R.: Open access series of imaging studies: longitudinal mri data in nondemented and demented older adults. *Journal of cognitive neuroscience* **22**(12), 2677–2684 (2010)
10. Muralidharan, P., Fletcher, P.: Sasaki metrics for analysis of longitudinal data on manifolds. In: CVPR. pp. 1027–1034. IEEE (2012)
11. Niethammer, M., Huang, Y., Vialard, F.: Geodesic regression for image time-series. In: MICCAI. pp. 655–662. Springer (2011)
12. Qiu, A., Younes, L., Miller, M., Csernansky, J.: Parallel transport in diffeomorphisms distinguishes the time-dependent pattern of hippocampal surface deformation due to healthy aging and the dementia of the alzheimer's type. *NeuroImage* **40**(1), 68–76 (2008)
13. Reuter, M., Schmansky, N., Rosas, H., Fischl, B.: Within-subject template estimation for unbiased longitudinal image analysis. *Neuroimage* **61**(4), 1402–1418 (2012)
14. Schiratti, J., Allasonniere, S., Colliot, O., Durrleman, S.: Learning spatiotemporal trajectories from manifold-valued longitudinal data. In: NIPS. pp. 2404–2412 (2015)
15. Singh, N., Hinkle, J., Joshi, S., Fletcher, P.: A vector momenta formulation of diffeomorphisms for improved geodesic regression and atlas construction. In: ISBI. pp. 1219–1222. IEEE (2013)
16. Singh, N., Hinkle, J., Joshi, S., Fletcher, P.: Hierarchical geodesic models in diffeomorphisms. *International Journal of Computer Vision* **117**(1), 70–92 (2016)
17. Tang, X., Holland, D., Dale, A., Younes, L., Miller, M.: The diffeomorphometry of regional shape change rates and its relevance to cognitive deterioration in mild cognitive impairment and alzheimer's disease. *Human brain mapping* **36**(6), 2093–2117 (2015)
18. Zhu, H., Kong, L., Li, R., Styner, M., Gerig, G., Lin, W., Gilmore, J.: Fdfts: functional analysis of diffusion tensor tract statistics. *NeuroImage* **56**(3), 1412–1425 (2011)